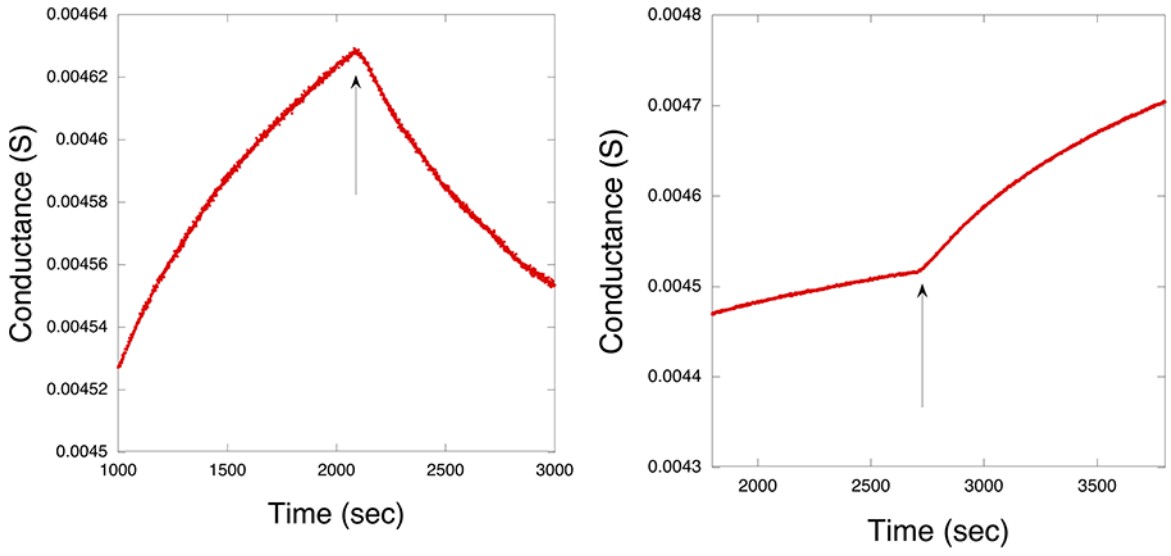

(a) **(b)**

Supplementary Figure 1 | The effect of changing pO_2 on the field-enhanced conductance

A constant potential of 0.4 V was maintained between electrodes 5 and 6 (the electrode configuration is shown in Fig. 1). (a) shows the conductance response when the chamber pO_2 was changed from 15 to 150 Torr at the time indicated by the arrow. (b) shows the response when the pO_2 was changed from 150 to 15 Torr, again at the time indicated by the arrow. In both cases, n-type behavior is observed.

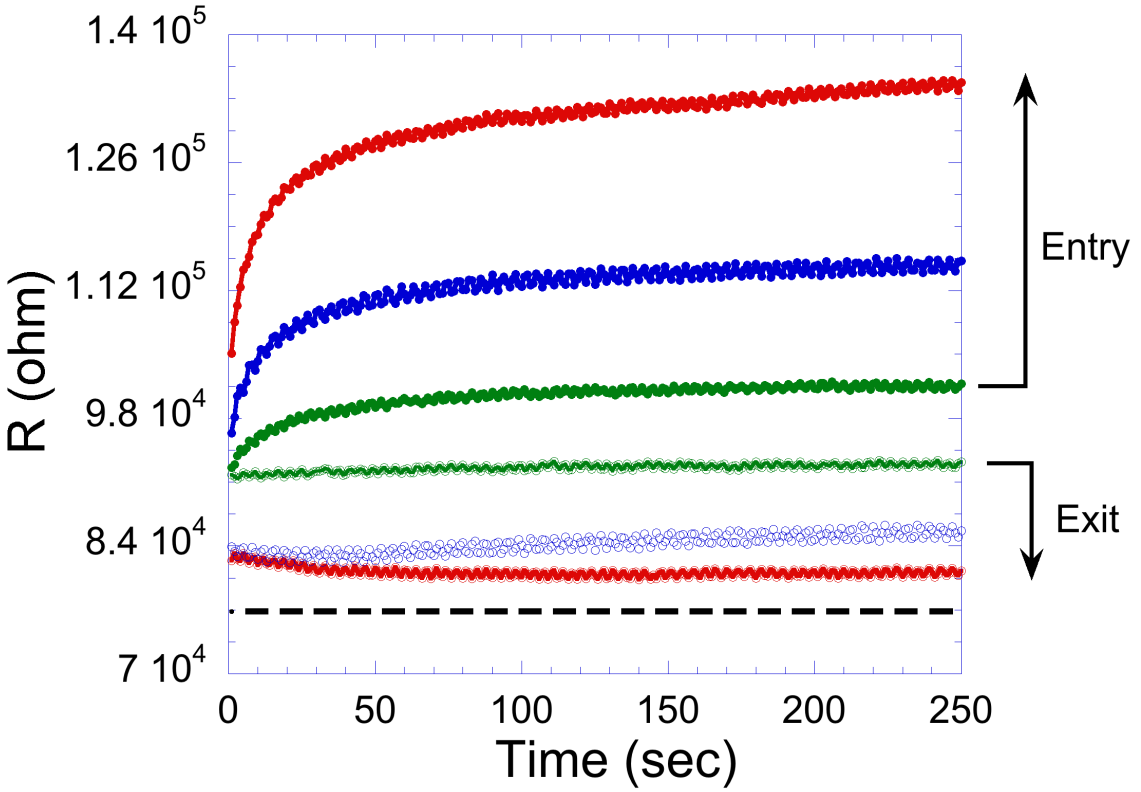

Supplementary Figure 2 | Development of contact resistances between YSZ and Ag end electrodes

At 370 °C for three different drive currents. Green curves: 1.5 μA; blue curves: 3 μA; red curves: 4.5 μA. At the negative current electrode (where oxygen entry occurs), the contact resistance increases systematically with increasing drive current. At the positive current electrode (where oxygen exit occurs), the resistance is small (and, for this sample, decreases systematically with increasing current). Measurements include the sample resistance measured between an end electrode and a Pt electrode on the top surface of the sample, R_{12} (shown as a dashed line; the electrode configuration is shown in Fig. 1).

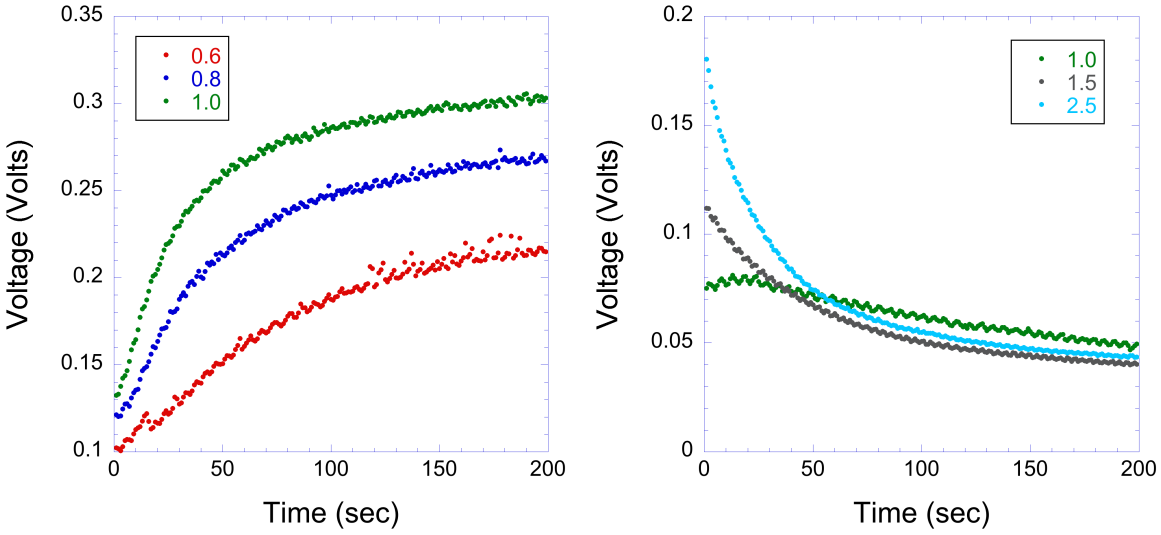

(a) **(b)**

Supplementary Figure 3 | Rectifying junctions at Ag/In_2O_3 contacts

(a) With electrode 7 positive, and electrode 1 negative, the voltage drop between electrodes 6 and 7 was measured, which included the positive Ag/In_2O_3 contact. Data are shown for three values of drive current flowing between electrodes 1 and 7 (electrode configuration shown in Fig. 1). The legend indicates the drive current magnitude, in μA. The voltage, and hence contact resistance, increased with time and with increasing current. This behavior is characteristic of the reverse direction of a rectifying junction. (b) With electrode 1 positive and electrode 7 negative, the voltage drop across electrodes 6 and 7 was measured with three values of drive current (shown in the legend, in μA; electrode configuration shown in Fig. 1). The voltage dropped with time as the sample resistance fell. There was no significant contact resistance. This is the forward direction of a rectifying junction. The initial rise and crossover behavior for the smallest current represent measurement uncertainty, probably resulting from prior sample measurement

history, with insufficient relaxation following the previous measurement. All measurements were made at 370 °C in $pO_2 =$ 1.5 Torr.

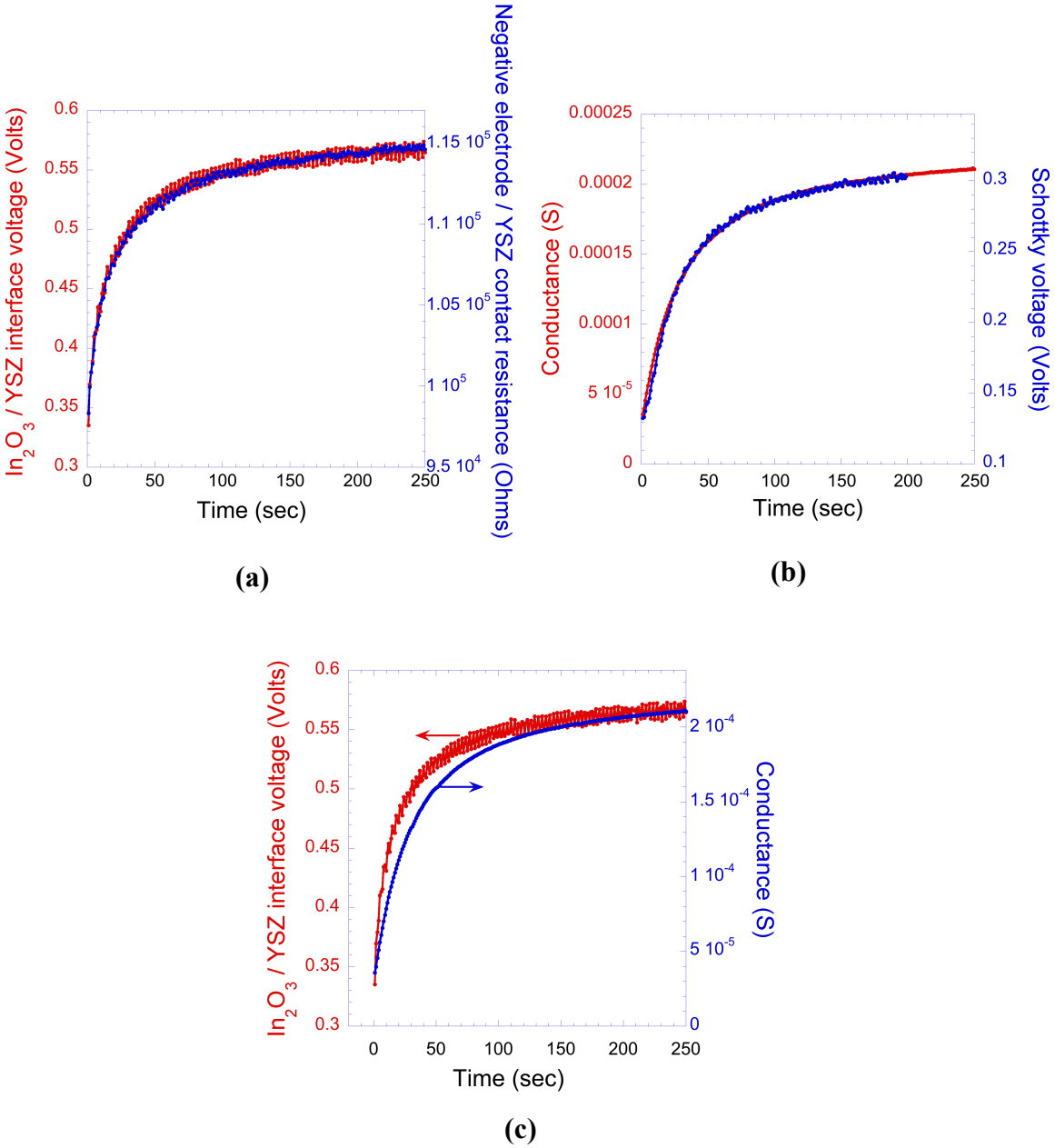

Supplementary Figure 4 | Interface time responses

(a) Comparison of the time response of the Ag negative current electrode / YSZ contact resistance (blue) and the voltage across the In_2O_3 / YSZ interface (red, measured using electrodes 2 and 2b, electrode configuration shown in Fig. 1). Since the YSZ contact resistance has a significant role in establishing the voltage across the film / substrate

interface, we expect the time dependences to be similar, as observed. (b) Time dependence of the Schottky voltage at the In_2O_3 / Ag positive current electrode compared to time dependence of the In_2O_3 conductance increase when an in-plane DC field is applied. The kinetics of the two phenomena are again very similar. (c) Time dependence of the development of the voltage across the YSZ / In_2O_3 interface, measured using electrodes 2-2b,compared to time dependence of the In_2O_3 conductance rise when an in-plane DC field is applied, measured using voltage pick-off electrodes 2 and 3 (electrode configuration is shown in Fig. 1). The kinetics are slightly faster for the voltage development, as expected, since diffusion of oxygen vacancies across the In_2O_3/YSZ interface occurs in response to the development of the voltage. All measurements were at 370 °C and pO_2 = 1.5 Torr.

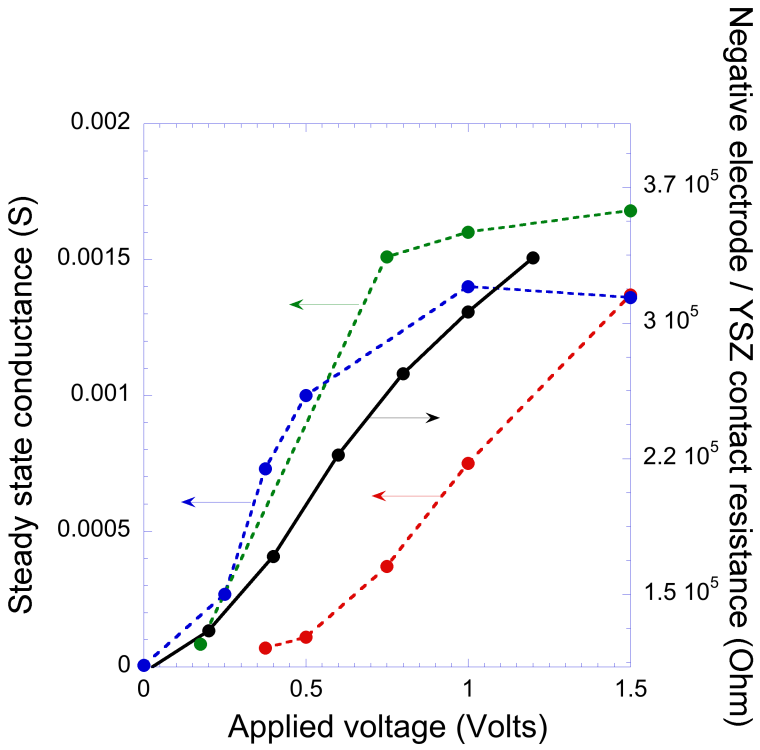

Supplementary Figure 5 | Comparison of sample conductance and interface resistance responses to applied field

In_2O_3-on-YSZ sample conductance at steady state when an in-plane DC field is applied versus applied voltage (measured using voltage pick-off electrodes 5 and 6, shown in Fig. 1), compared to the Ag negative current electrode / YSZ contact resistance at steady state versus applied voltage. Similar behaviors are observed. The steady state conductance shows a weak dependence on pO_2. Conductance measurements were made at 150 Torr (red), 0.15 Torr (blue) and 0.0015 Torr (green). All measurements were at 370 °C.

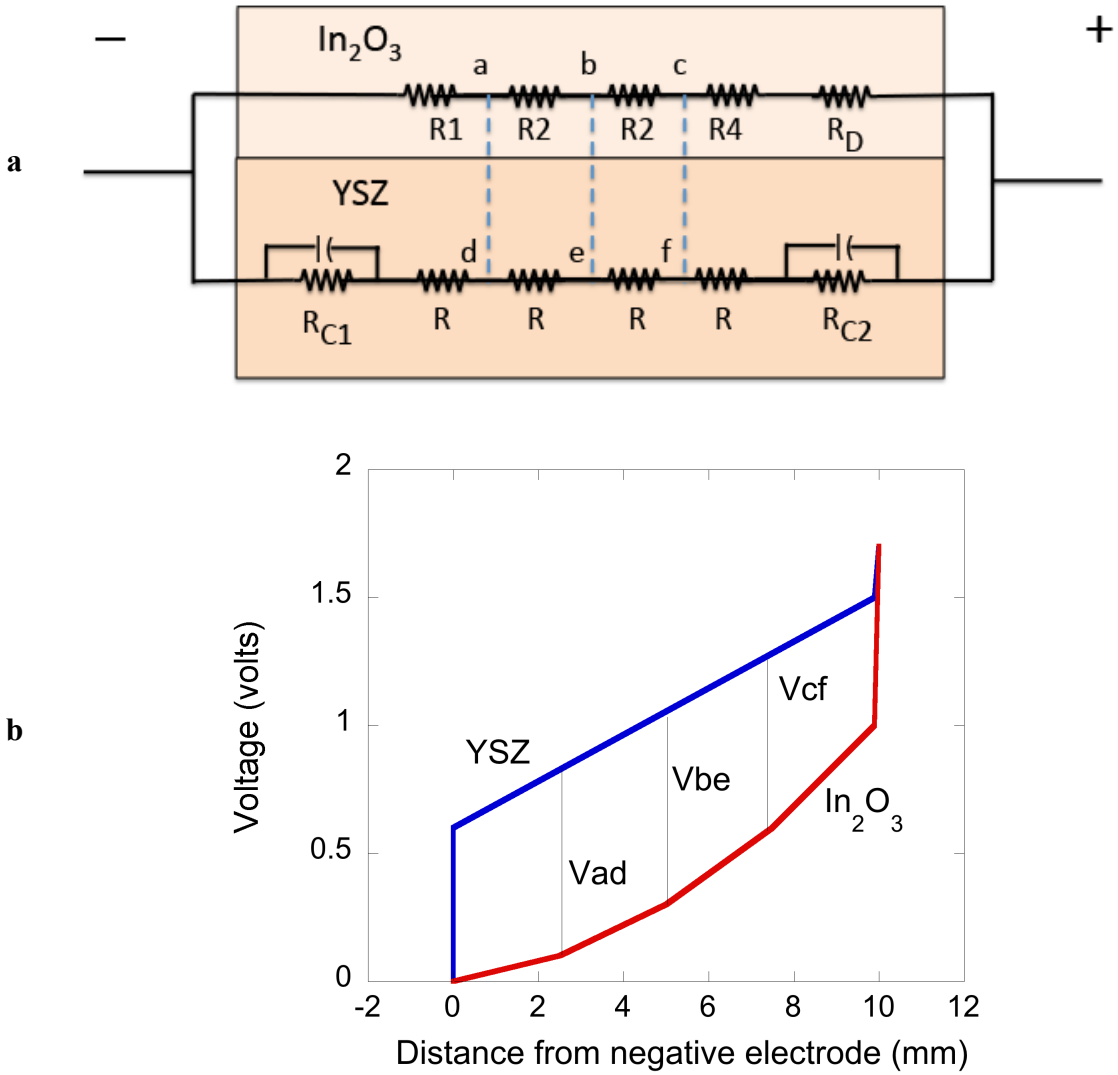

Supplementary Figure 6 | Approximate equivalent circuit and corresponding voltage profile

(a) Approximate equivalent circuit at steady state when an in-plane DC voltage is applied (transient behavior is not represented). The RC elements represent the Ag current electrode / YSZ contacts and the resistor R_D represents the reverse bias diode at the Ag current electrode / In_2O_3 contacts. The resistors R represent the YSZ sample resistance.

(b) The corresponding voltage profile for YSZ (blue) is determined by the contact resistances and by the sample resistivity, which does not vary with distance across the sample. For In_2O_3 (red), a Schottky resistance appears at the positive current electrode and there is a gradient in resistivity between the current electrodes, so the field profile is not linear. That is, R4 > R3 > R2 > R1. With a DC voltage across the sample, there will be a voltage drop between YSZ and In_2O_3, with the YSZ bulk at higher potential than the In_2O_3. The voltages Vad > Vbe > Vcf.

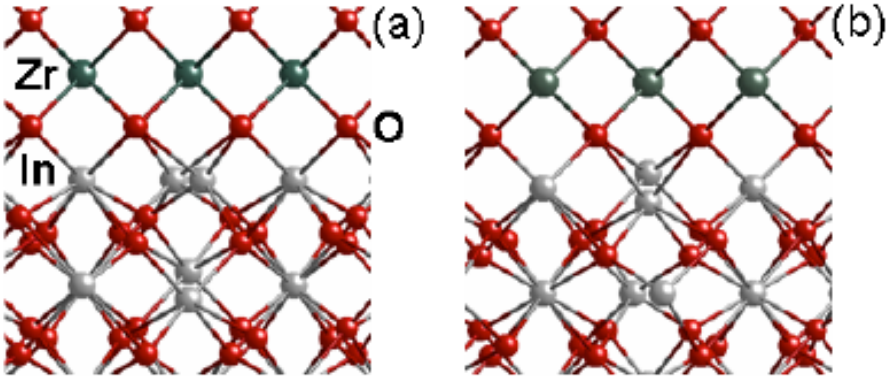

Supplementary Figure 7 | Side view of the optimized In_2O_3-ZrO_2 interface structure

(a) The "flat" interface that contains two types of In sites (8b and 24d) in the cation plane immediately adjacent to the shared oxygen interface plane is shown. (b) The "buckled" interface with only one type of In atom (24d) in the cation plane immediately adjacent to the shared oxygen interface plane is shown.

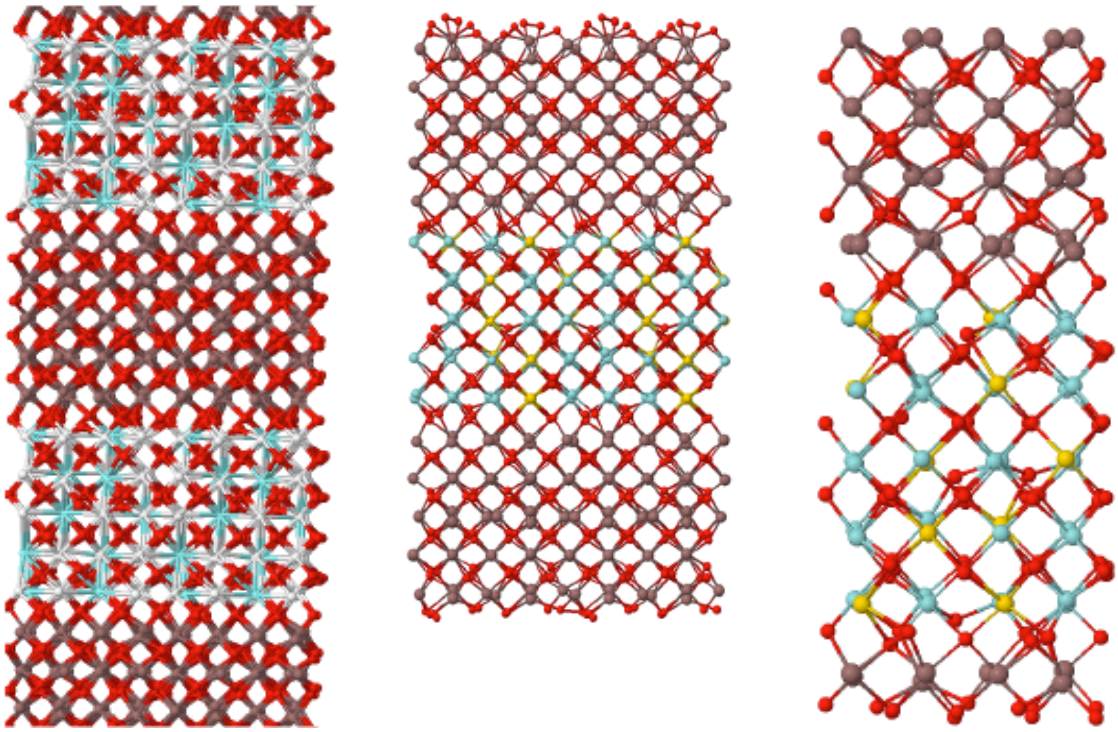

a **b** **c**

Supplementary Figure 8 | Side view of optimized interface structures

(a) (001) initial In_2O_3-ZrO_2 interface structure shown in a 2x2x2 supercell (with stoichiometry $In_{40}Zr_{40}O_{140}$), (b) O-deficient In_2O_3-YSZ interface structure (with stoichiometry $In_{40}Zr_{30}Y_{10}O_{131}$), (c) enlarged view of the interface region shown in b. Colors: Y = yellow, Zr = blue, O = red, In = brown.

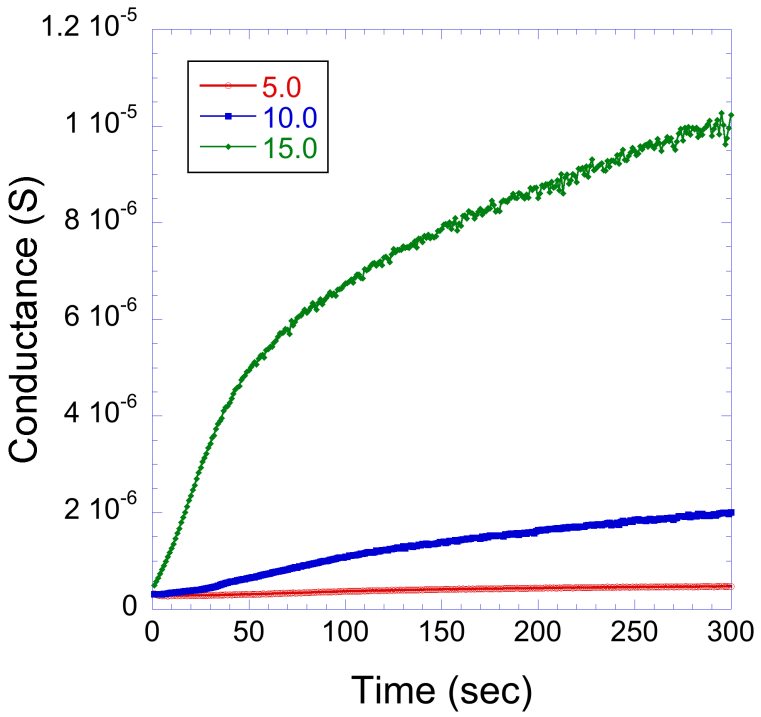

Supplementary Figure 9 | Conductance versus time for an epitaxial WO_3 film on a (001) YSZ substrate

Measured under constant field conditions (two electrode measurement at 330° C and pO_2 = 1.5 Torr, with Ag end electrodes). Measurements were obtained at the potentials indicated in the legend (in units of Volts). With 15 V applied between the end electrodes, the conductance was observed to rise by more than a factor-of-30.

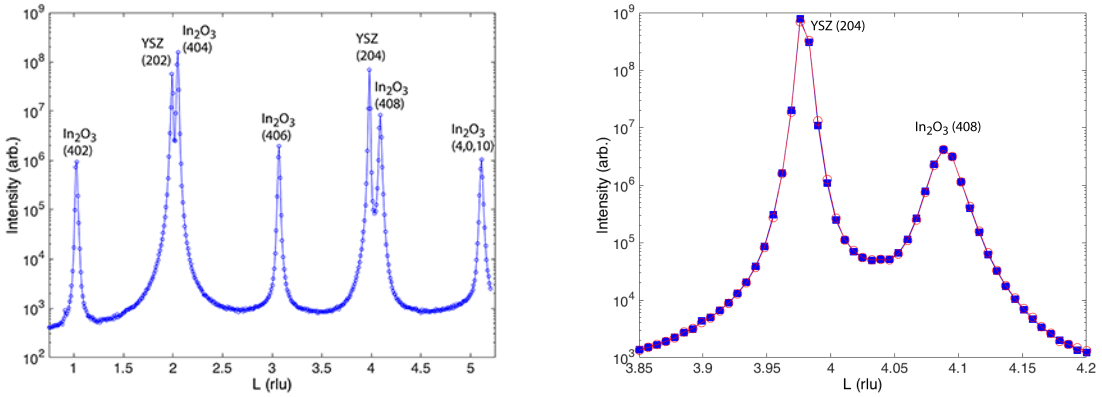

a **b**

Supplementary Figure 10 | In-situ synchrotron x-ray characterization

(a) Scan of the [20L] (YSZ reciprocal space units) direction of an In_2O_3 / YSZ epitaxial thin film heterostructure, demonstrating the cube-on-cube orientation relationship of the film to the substrate. (b) Scan of the (204) YSZ and (408) In_2O_3 Bragg peaks prior to and during application of a small DC field oriented in the plane of the film. While simultaneous electrical measurements showed a field-induced conductance increase, neither the in-plane nor out-of-plane components of the film and substrate lattice parameters changed by a measurable amount. Blue = 0 *V* applied, Red = 2.0 *V* applied. Sample temperature = 300°C.

Supplementary Table 1 | Film thickness-dependent behavior

Thickness (nm)	$G_o \times \frac{L}{A}$ (S/cm)	$G_\infty \times \frac{L}{A}$ (S/cm)
4	10	600
16	14	300
70	11	60

The measured conductivities of three samples with different thickness In_2O_3 films were compared at 370° when a constant 1 V potential was maintained between the voltage pick-off electrodes. G_o is the initial measured conductivity when the field is applied, G_∞ is the field-enhanced conductivity at steady state, L is the distance between the pick-off electrodes, and A is the film thickness. The comparison indicates that the enhanced conduction resulting from the field application is highly localized to the In_2O_3 / YSZ heterointerfacial region.

Supplementary Note 1 | Additional Electrical Characterization

In_2O_3 is an oxide semiconductor, exhibiting n-type conductivity. This behavior is confirmed in Supplementary Figure 1, where the effect of changing pO_2 on the field-enhanced conductance is shown. Increasing the pO_2 resulted in a decrease in the field-induced conductance value, while decreasing the pO_2 resulted in increasing conductance. Similar behavior was observed with samples equilibrated in oxygen partial pressures controlled between 0.0015 and 150 Torr O_2. Changes in conductance due to changing pO_2, however, were much smaller than the electric field-induced changes in conduction observed. Thus, unless otherwise indicated, the measurements described in this paper were carried out on samples equilibrated in 1.5 Torr O_2.

For electrical measurements of the thin film heterostructures, the conductance of the YSZ substrate is small compared with that of the film. For the bare substrate, the resistance measured between pick-off electrodes 2 and 6 (R_{26}, with the electrode configuration shown in Fig. 1) varies between 650,000 Ω at 370 °C and 2.7 MΩ at 330 °C and is independent of measurement voltage. Bare YSZ substrates show no field-induced changes in conductivity with time.

Zero field conductances of different In_2O_3/YSZ heterostructures varied substantially, depending on film thickness, temperature, pO_2, and perhaps on subtle differences in preparation technique, which can result in different levels of impurity concentration in the In_2O_3 and thus varying levels of electron doping. The highest zero field resistance measured at 370 °C was R_{26} = 430,000 Ω with zero applied field. (With field, this dropped more than two orders of magnitude.)

Contact resistances were characterized at both the positive and negative Ag/YSZ (or Pt/YSZ) contacts. The contact resistances (painted contacts) can be quite variable, and are subject to electrode damage. For example, if the in-plane voltage is excessive (a few volts), oxygen transport through the sample can cause electrode damage, especially of the oxygen exit electrode, increasing the contact resistance.

For the current electrode / YSZ contacts, Supplementary Figure 2 shows measurements of contact resistance, with increasing drive current (through electrodes 1 and 7), from a bare YSZ sample. At the negative current electrode (where oxygen entry occurs), the contact resistance increases systematically with increasing drive current. The resistance at the positive current electrode (where oxygen exit occurs) is substantially smaller than the resistance at entry. (The small resistance at zero field actually decreases systematically with increasing current.) The measurements include the sample resistance R_{12} between electrodes 1 and 2. This resistance is given by the dashed line.

For Ag/In_2O_3 contacts, the resistance at the positive contact develops with time as shown in Supplementary Figure 3a; the figure shows the voltage measured with different values of constant current. Supplementary Figure 3b shows measurements at the negative electrode. Here, the voltage drops with time as the sample resistance falls. The falling resistance is attributable to the In_2O_3 resistance between electrodes 6-7. There is no significant contact resistance. This behavior is characteristic of a rectifying junction.

Supplementary Figure 4a shows a comparison of the time responses of the Ag/YSZ contact resistance and the development of voltage across the In_2O_3 / YSZ interface. Since the YSZ / negative current electrode contact resistance contributes significantly to the development of the voltage across the In_2O_3 / YSZ interface, we

expect the time dependences of these two quantities to be essentially the same, as observed. Likewise, Supplementary Figure 4b shows the time dependence of the Schottky voltage that develops at the positive current electrode / In_2O_3 electrode, compared to the time dependence of the In_2O_3 conductance. Again the time responses are the same, providing further support to our conclusion that the field-induced conductance increases observed arise because of the development of contact resistances at the negative current electrode / YSZ and positive current electrode / In_2O_3 interfaces. An additional comparison can be made of the kinetics of the voltage development across the In_2O_3 / YSZ interface and that of the sample conductance change when a field is applied. Supplementary Figure 4c shows the time dependence of the voltage between electrodes 2 and 2b, compared to the time dependence of the In_2O_3 conductance measured using voltage pick-off electrodes 2 and 3. We observe that the conductance change kinetics are slightly slower than voltage kinetics. This is reasonable, since the conductance change occurs in response to the development of the voltage across the interface. The In_2O_3/YSZ measurements in Supplementary Figures 4a-4c were made on the same sample at 370 °C, under constant current conditions.

Supplementary Figure 5 shows the In_2O_3 / YSZ heterostructure conductance at steady state versus applied voltage, over-plotted with the negative current electrode /YSZ contact resistance at steady state versus applied voltage. Again, since the conductance increase follows the rise in contact resistance, we expect the functional dependence of these separate measurements to be closely related (as observed). The steady state conductance shows only a very weak dependence on pO_2, suggesting that the oxygen vacancy doping levels at steady state with a field applied are predominately controlled by

the field-induced voltage that develops across the In_2O_3 / YSZ interface rather than by the pO_2.

Supplementary Note 2 | Interfacial space-charge region

To estimate the extent of the interfacial space-charge region in In_2O_3, we used the expression for the Debye length, $L_D = sqrt[(\varepsilon K_B T)/(n_0 e^2)]$, where ε and n_0 are the dielectric constant and carrier concentration for the undoped ($E = 0$) In_2O_3 film, K_B is the Boltzmann constant, and T is the absolute temperature. Using $\sigma = n_0 e \mu$, with $\sigma = 2$ S/cm (e.g., Fig 2) and $\mu = 50$ cm^2/V-sec,[1,2] we obtain $n_0 = 3 \times 10^{17}$ /cm^3. Using the value 8.9 ε_0 for the dielectric constant of In_2O_3 films reported by Hamburg and Granqvist[3], we obtain $L_D = 11$ nm. We can also make a rough estimate of the field strength at the interface. For a vertical voltage of 0.5 volts an approximate screening length of 11 nm, we estimate the field strength is on the order of 5×10^5 volts/cm.

Supplementary Note 3 | Approximate equivalent circuit

An approximate equivalent circuit, representing the electron and ion conduction network, at steady state, is presented in Supplementary Figure 6a. The RC elements represent the Ag (or Pt)/YSZ contacts and resistor R_D represents the reverse bias diode at the Ag (or Pt) / In_2O_3 contact. The resistors R represent the YSZ sample resistance, which is unchanged by the field application. The resistors R1 through R4, represent the In_2O_3 resistance. All four of these resistances are smaller than they would be prior to applying the field. The voltage profile for YSZ (blue, Supplementary Figure 6b) is determined by the contact resistances and by the sample resistance. The YSZ substrate resistivity (or

resistance per unit length) does not vary with distance laterally across the sample. For In_2O_3 (red), there is a gradient in resistance between end electrodes, so the field profile is not linear. That is, R4 > R3 > R2 > R1. With a DC voltage across the end electrodes, there is a voltage drop between YSZ and In_2O_3. The vertical voltages Vad > Vbe > Vcf. Since there is minimal resistance at the negative Ag (or Pt)/ In_2O_3 electrode, and R_{C1} is large, the voltage at YSZ is positive relative to the In_2O_3 (providing the driving force to move oxygen ions from In_2O_3 to YSZ). With applied voltage across the end electrodes, the In_2O_3 sample resistance changes (falls) and a conductance gradient develops. Also, the rectifying junction (diode) at the positive Ag (or Pt)/ In_2O_3 electrode develops after the voltage is applied. This time dependent behavior is not represented in the equivalent circuit.

Supplementary Note 4 | X-Ray Diffraction Measurements

Synchrotron X-ray diffraction measurements were carried out at the Advanced Photon Source at Argonne National Laboratory. A 75 nm thick In_2O_3 film grown on (001) YSZ was examined at 300°C before and during application of an in-plane DC 4 V/cm field (2 V were applied between the end electrodes, which were separated by 5 mm). Scans such as Supplementary Figure 10a confirmed the cube-on-cube orientation relationship between the film and substrate. With zero field applied, this film was observed to be partially relaxed in-plane; the in-plane In_2O_3 lattice parameter was 0.6% smaller than that of the YSZ substrate, indicating a small tensile strain. (If fully relaxed, the in-plane lattice parameter would have been 1.6 % smaller than that of the substrate). The out-of-plane In_2O_3 lattice parameter was reduced by 0.48 %, relative to bulk In_2O_3,

due to the Poisson effect. As seen in Supplementary Figure 10b, when an in-plane DC field was applied, while monitoring the positions of one YSZ and one In_2O_3 Bragg peak, there was no measurable change in the in-plane or out-of-plane lattice parameter of either material (the measurement resolution was ~ 0.02%). Simultaneous electrical measurements indicated the expected field-induced conduction enhancement. As expected, the change in oxygen vacancy doping with field, while large enough to cause a significant conductance change, was inadequate to cause a measurable lattice parameter change, since the field enhanced vacancy concentration is ~ 10^{18} cm^{-3}, or about one vacancy per 10^5 oxygen atoms (see Space Charge discussion in Supplementary Note 2).

Supplementary References

1. H. Ohta, M. Orita, M. Hirano, H. Tanji, H. Kawazoe and H. Hosono, Highly electrically conductive indium-tin-oxide thin films epitaxially grown on yttria-stabilized zirconia (100) by pulsed-laser deposition, *Appl. Phys. Lett*., **76**, 2740 (2000).
2. A. Dixit, Raghava, P. Panguluri, C. Sudakar, P. Kharel, P. Thapa, I. Avrutsky, R. Naik, G. Lawes, and B. Nadgorny, Robust room temperature persistent photoconductivity in polycrystalline indium oxide films, *Appl. Phys. Lett*., **94**, 252105 (2009).
3. I. Hamburg and C. G. Granqvist, Evaporated Sn-doped In_2O_3 films: Basic optical properties and applications to energy-efficient windows, *J. Appl. Phys*. **60**, R123 (1986); Dielectric function of "undoped" In_2O_3, *Thin Solid Films* **105**, L83-86 (1983).

4. G. P. Wirtz and H. P. Takiar, **64**, Oxygen diffusion in vapor-deposited indium oxide films, *J. Am. Ceram. Soc*., 748 (1981)

5. Y. Ikuma, M. Kamiya, N. Okumura, I. Sakaguchi, H. Haneda and Y. Sawada, Oxygen diffusion in single-crystal In_2O_3 and tin-doped In_2O_3, *J. Electrochem. Soc*., Vol. 145, No. 8, 2910 (1998).

6. Y. Ikuma and T. Murakama, Oxygen tracer diffusion in polycrystalline In_2O_3, *J. Electrochem. Soc*., Vol. 143, No. 8, 2698 (1996).